JOC The Journal of Organic Chemistry

Article

pubs.acs.org/joc

Studies of (−)-Pironetin Binding to α-Tubulin: Conformation, Docking, and Molecular Dynamics

Angel E. Bañuelos-Hernández,[†] José Alberto Mendoza-Espinoza,[†] Rogelio Pereda-Miranda,[‡] and Carlos M. Cerda-García-Rojas*[,†]

[†]Departamento de Química y Programa de Posgrado en Farmacología, Centro de Investigación y de Estudios Avanzados del Instituto Politécnico Nacional, A. P. 14-740, México D. F. 07000, Mexico

[‡]Departamento de Farmacia, Facultad de Química, Universidad Nacional Autónoma de México, Circuito Exterior Ciudad Universitaria, México D. F. 04510, Mexico

Supporting Information

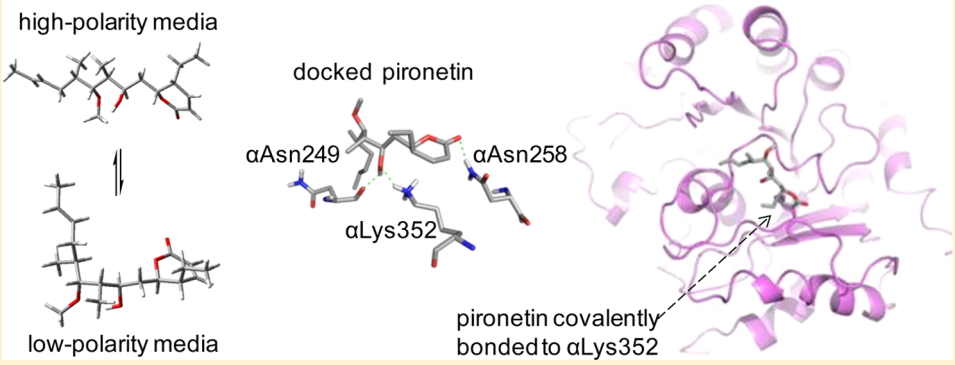

ABSTRACT: A comprehensive conformational analysis for the anticancer agent pironetin (**1**) was achieved by molecular modeling using density functional theory calculations at the B3PW91/DGTZVP level in combination with calculated and experimental $^{1}H-^{1}H$ coupling constants comparison. Two solvent-dependent conformational families (*L* and *M*) were revealed for the optimum conformations. Docking studies of the pironetin−tubulin complex determined a quantitative model for the hydrogen-bond interactions of pironetin through the αAsn249, αAsn258, and αLys352 amino groups in α-tubulin, which supported the formation of a covalent adduct between the αLys352 and the β carbon atom of the α,β-unsaturated lactone. Saturation-transfer difference NMR spectroscopy confirmed that pironetin binds to tubulin, while molecular dynamics exposed a distortion of the tubulin secondary structure at the H8 and H10 α-helices as well as at the S9 β-sheet, where αLys352 is located. A large structural perturbation in the M-loop geometry between the αIle274 and αLeu285 residues, an essential region for molecular recognition between α−α and β−β units of protofilaments, was also identified and provided a rationale for the pironetin inhibitory activity.

INTRODUCTION

The α,β-tubulin heterodimer is the basic structural constituent of microtubules and one of the leading targets for cancer therapy due to its relevant role in cellular replication.[1] Subsequently, substances which interfere with its polymerization and depolymerization process are candidates for drug development.[2] Pironetin (**1**) (Figure 1),[3−5] isolated from the fermentation broths of *Streptomyces prunicolor* PA-48153 and *Streptomyces sp.* NK 10958,[6] is a potent inhibitor of tubulin assembly. This polyketide, as well as its 7′,8′-epoxide and demethoxylated derivatives,[4] containing the pharmacophoric alkenyl-5,6-dihydro-2*H*-pyran-2-one moiety,[7] showed antiproliferative activity against various cancer cell lines including HL-60 human myeloid leukemia.[4] Although most tubulin-interacting agents attach to the β-unit, pironetin covalently binds to the α-unit at Lys352, which is located in the β-sheet 9 strand at the entrance of a small pocket and facing the β-tubulin unit of the next dimer, resulting in microtubule destabilization.[5] This bioactive compound has become the focal point of a series of studies in relation to its asymmetric and enantioselective total syntheses[8] and was found to be effective against cell lines

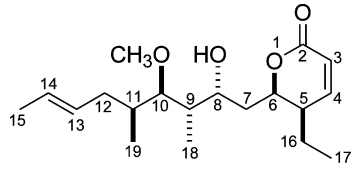

1

Figure 1. Chemical structure of pironetin (**1**).

Received: September 10, 2013
Published: April 11, 2014

   dx.doi.org/10.1021/jo500420j | J. Org. Chem. 2014, 79, 3752−3764

resistant to microtubule-targeted drugs and multidrug-resistant cells with mdr1 gene expression.[9] Pironetin also showed cancer-cell-specific apoptosis as well as inhibition of in vivo angiogenesis[10] and was used as a model compound to explore apoptotic mechanisms.[11]

Several studies on the design, synthesis, and biological evaluation of pironetin analogues have been published, including modifications to simplify the structure and enhance its lipophilicity.[12] More recently, work on synthesis of pironetin analogues hybridized with combretastatin derivatives and evaluation of their cytotoxic activity was reported.[13] A previous study characterized the pironetin binding site by systematic alanine scanning demonstrating that pironetin covalently binds to α-tubulin at αLys352.[4] Quantitative models for the conformational behavior as well as the molecular dynamics of pironetin's mode of interaction with tubuline in solution have not been explored. This work describes the conformational analysis of pironetin on the basis of density functional theory (DFT) calculations compared with detailed ^{1}H−^{1}H NMR coupling constant analysis. These studies present the conformational preferences and three-dimensional features of pironetin for the generation of the α-tubulin-ligand interaction models and their molecular dynamics.

RESULTS AND DISCUSSION

Conformational Analysis. Because of the large number of rotating bonds and the capacity of pironetin to form inter- and intramolecular hydrogen bonds, its conformational analysis presented a significant challenge. Construction of minimum energy molecular models was based on the Spartan[14] program and then followed by an extensive conformational search using the Monte Carlo method,[15] applying the MMFF94 force field[16] with an energy window established from 0 and 15 kcal/mol. After analysis of the geometries and removal of duplicates, a group of 967 conformers was obtained and followed by DFT geometry optimization at the B3LYP/6-31G(d) level[17] yielding 107 distinct conformers within the first 4.5 kcal/mol. Geometrical optimization followed using the B3PW91 functional and the DGTZVP[18] basis set as implemented in the Gaussian program[19] to afford 53 conformers with relative energies ranging from 0 to 3 kcal/mol. Thus, the omission of any essential conformer due to the high degree of torsional freedom of **1** was avoided. Figure 2 shows the eight most stable conformers of pironetin representing approximately 70% of the conformational population.

Theoretical Coupling Constant Calculations. NMR parameters for each structure were calculated using the Gaussian program.[19] The gauge-included atomic orbital (GIAO) method provided the shielding tensors and the coupled perturbed Kohn−Sham method calculated the ^{1}H−^{1}H NMR coupling constant terms, i.e., the Fermi contact, the spin-dipole, the diamagnetic spin−orbit, and the paramagnetic spin−orbit.[20] The four terms of each of the ^{1}H−^{1}H vicinal and geminal coupling constants ($J_{H,H}$) calculated at the B3PW91/DGTZVP level[21] were combined and are listed for each conformer in Table S1 (Supporting Information). The $\Delta G = -RT \ln K$ equation provided the population for each conformer by taking into consideration a cyclic equilibrium among the selected ones. Each coupling value was Boltzmann-weighted, taking into account the DFT population to integrate the population-averaged coupling constants. A scaling factor, obtained in previous work,[22] was applied to the DFT-calculated $J_{H,H}$ in vacuo showing a very good correlation with the experimental couplings measured in $CDCl_3$ (Table 1) with the exception of the vicinal coupling between H-9 and H-10 ($J_{9,10}$). Molecular models were able to mimic the conformation of the pyrone ring including the initial portion of the alkyl chain (O1−C2−C3−C4−C5−C6−C7-C8), the ethyl chain (C16−C17), plus the terminal alkenyl moiety (C11−C12−C13═C14−C15), but not the behavior of the central region of the alkyl chain (C8−C9−C10−C11). A detailed analysis involving the measurement of the ^{1}H NMR spectrum in a solvent with a differing dielectric constant was required to explain the origin of such a difference. In CD_3OD, the difference between the theoretical and experimental $J_{9,10}$ became larger and a noticeable modification occurred in $J_{10,11}$ (Table 2).

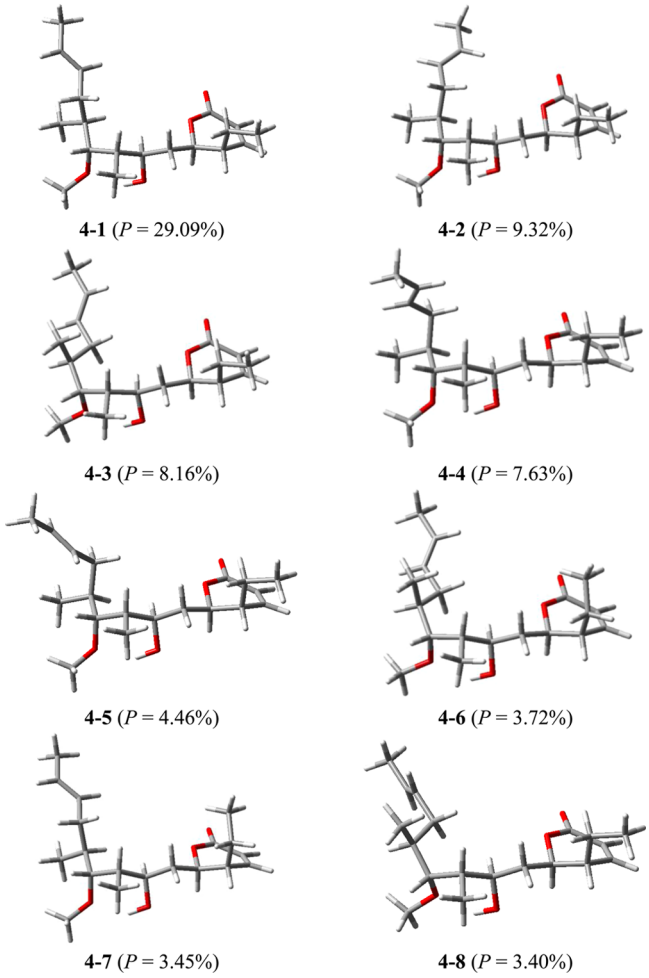

Figure 2. Most relevant conformers of pironetin calculated in vacuo at the DFT B3PW91/DGTZVP level.

Two conformational families can be identified among the numerous pironetin rotamers (Table 1). The first group is formed by those conformers adopting an *L* arrangement in the alkenyl side chain and presenting an intramolecular hydrogen bond between the hydroxyl group at C-8 and the methoxyl group at C-10 (Figure 3). The second one, named herein as *M*, is formed by those conformers in which the alkenyl side chain is extended in a zigzag arrangement with the hydroxyl and methoxyl groups oriented toward opposite faces (Figure 3). *L*-Type conformations prevailed in vacuo or in such aprotic low-polar solvents as $CHCl_3$ because of the O(8)−H(8)---O(10) intramolecular hydrogen bond. The *M*-type, sterically more favored, predominated in polar solvents as CH_3OH where they

dx.doi.org/10.1021/jo500420j | J. Org. Chem. 2014, 79, 3752−3764

Table 1. DFT Calculated and Experimental ^{1}H−^{1}H Coupling Constants of Pironetin

^{1}H−^{1}H	J_{calcd} [a]	J_{exp} [b]	^{1}H−^{1}H	J_{calcd} [a]	J_{exp} [b]
3,4	9.95	9.80	7*proS*,8	1.35	2.70
4,5	6.08	6.00	8,9	1.28	1.70
5,16*proR*	9.54	9.70	9,10	1.57	4.00
5,16*proS*	4.54	4.70	10,11	7.83	6.60
16*proR*,16*proS*	−13.82	−13.60	11,12*proR*	9.20	8.00
5,6	3.77	3.50	11,12*proS*	2.91	4.30
6,7*proR*	1.55	2.50	12*proR*,12*proS*	−14.09	−13.50
6,7*proS*	9.54	9.90	12*proR*,13	8.39	7.30
7*proR*,7*proS*	−13.62	−13.70	12*proS*,13	5.58	6.40
7*proR*,8	9.67	9.70	13,14	14.73	14.80

[a]Theoretical coupling constants (in hertz) were calculated at the B3PW91/DGTZVP level for the 53 most stable optimized structures. Coupling constants were Boltzmann-averaged using the $\Sigma_i J^i \times P^i$ equation, where J^i is the coupling constant value for each conformer and P^i is the population for the *i*th conformation calculated from the relative Gibbs free energies at 298 K and 1 atm. The averaged coupling constants were scaled with factors: $f_{H(sp3)-H(sp3)}$ = 0.910; $f_{H(sp3)-H(sp2)}$= 0.929, and $f_{H(sp3)-H(sp3)}$= 0.977. [b]In hertz obtained by nonlinear fit of the experimental ^{1}H NMR spectrum to the simulated spectrum (for full details, see Table S1, Supporting Information).

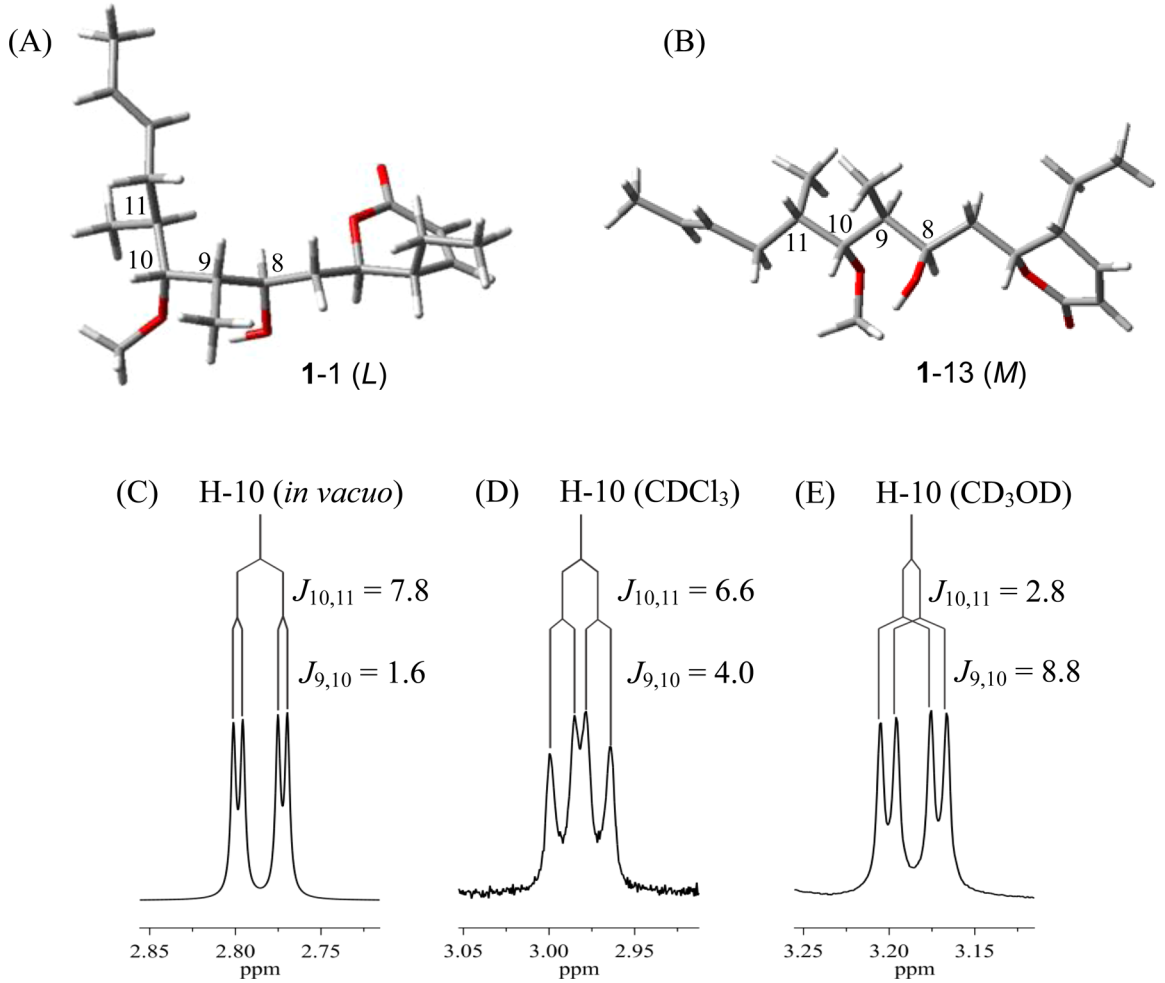

Figure 3. Top: representative minimum energy structures for the two conformational families of pironetin. (A) Molecular model for an *L*-type conformer (**1**-1) and (B) molecular model for an *M*-type conformer (**1**-13). Bottom: H-10 coupling constants variation ($J_{9,10}$ and $J_{10,11}$) as a function of the media reflects changes in the conformational populations. (C) H-10 in vacuo (mainly *L*-type conformers), (D) H-10 in $CDCl_3$ (coexistence of both *L*- and *M*-type conformers), and (E) H-10 in CD_3OD (mainly *M*-type conformers).

were stabilized by intermolecular hydrogen bonds (Tables S2 and S3, Supporting Information). In fact, the observed conformation in the solid state[6] corresponded to the *M*-type since the molecular crystal packing involved the intermolecular hydrogen bonds.

Thus, the theoretical values for pironetin $J_{9,10}$ = 1.6 Hz and $J_{10,11}$ = 7.8 Hz showed that in vacuo most conformers belong to the *L*-type family (Table 2), while the $J_{9,10}$ = 4.0 Hz value in $CDCl_3$ indicated that there is an important contribution of both conformational families. According to the following equations,

dx.doi.org/10.1021/jo500420j | J. Org. Chem. 2014, 79, 3752−3764

Table 2. $^1H-^1H$ Coupling Constants (Hz) for the C9−C10−C11 Fragment in Several Media and the *L*:*M* Conformational Ratio

media	$J_{9,10}$ (Hz)	$J_{10,11}$ (Hz)	*L*:*M* ratio (%)[a]
in vacuo (DFT)	1.6	7.8	93:7
$CDCl_3$	4.0	6.6	64:36
CD_3OD	8.8	2.8	7:93

[a]Calculated taking into account the $J_{9,10}$ and $J_{9,10}$ theoretical couplings for conformers **4**-1 and **4**-13.

L-type conformers exist in 64% while *M*-type are present in 36%.

$$J = \%L(J_{\text{calc-}L}) + \%M(J_{\text{calc-}M})\%L + \%M = 100\%$$

In CD_3OD, the conformational population shifted toward the *M*-type conformers to an estimated 93% from the observed coupling constant ($J_{9,10}$ = 8.8 Hz). To explore the solvent influence on the energy values as well as on the types *L* and *M* conformers, the solvation energy for one representative conformer of each group, using $CHCl_3$ and CH_3OH, was calculated, i.e., **1**-1 (for *L*-type) and **1**-13 for (for *M*-type). Polarizable continuum model (PCM)[23] provided the calculations. The corresponding values are included in Table 3

Table 3. Free Energy for Conformers 1-1 and 1-13 of Pironetin in Several Media[a]

conformer	$\Delta G_{\text{in vacuo}}$	$\Delta G_{\text{in vacuo}} + \Delta G_{CHCl_3}$	$\Delta G_{\text{in vacuo}} + \Delta G_{CH_3OH}$
1-1 (*L*)	0.000	−3.651	−30.697
1-13 (*M*)	1.753	−2.275	−32.085
$\Delta\Delta G$	1.753	1.375	−1.388

[a]In kcal/mol calculated with the polarizable continuum model at the DFT B3PW91/DGTZVP level of theory. The free energy absolute value for conformer **1**-1 in vacuo is −654901.593 kcal/mol.

together with the free energy values for comparison. The free energy difference between conformers **1**-1 (*L*-type) and **1**-13 (*M*-type) in $CHCl_3$ ($\Delta\Delta G_{CHCl_3}$ = 1.375 kcal/mol) reflects a slightly increased preference for conformer **1**-13 in respect to the free energy difference in vacuo ($\Delta\Delta G_{\text{in vacuo}}$ = 1.753 kcal/mol), although in both cases the predominant conformer is **1**-1 (*L*-type). In CH_3OH, the free energy difference indicated a significant prevalence of the *M*-type conformation over the *L*-type ($\Delta\Delta G_{CH_3OH}$ = −1.388 kcal/mol). The energy difference (3.14 kcal/mol) between $\Delta\Delta G_{\text{in vacuo}}$ and $\Delta\Delta G_{CH_3OH}$ corresponded to that for a hydrogen bond. The results indicated that such a value could correspond to the energy associated with gaining two intermolecular hydrogen bonds with the solvent (CH_3OH) in **1**-13 and losing one intramolecular hydrogen bond due to the conformational change of going from **1**-1 to solvated **1**-13.

Spectral Simulation. The ^1H NMR spectrum (300 MHz) of pironetin shows a complex pattern in which H-9 and H-11 methine signals overlap with H-7, H-12 and H-16 methylene signals, generating high-order spin systems. Therefore, precise chemical shifts and coupling constants were simulated by multiple iterations of the spectral parameters using the MestReNova program.[24] Under irradiation of H-10 at δ 2.98 ppm, H-9 and H-11 signals were simplified permitting a simulated trace similar to the experimental spectrum with a root-mean-square error of 0.41 Hz (Figure 4). At this point, H-10 was included in the simulation data set, completing the spectral simulation of pironetin resulting in a root-mean-square error of 0.37 Hz. The final spectral parameters for the 30 nuclei are listed in Table 4. The comparison for the simulated and experimental spectra is shown in Figure S1 (Supporting Information).

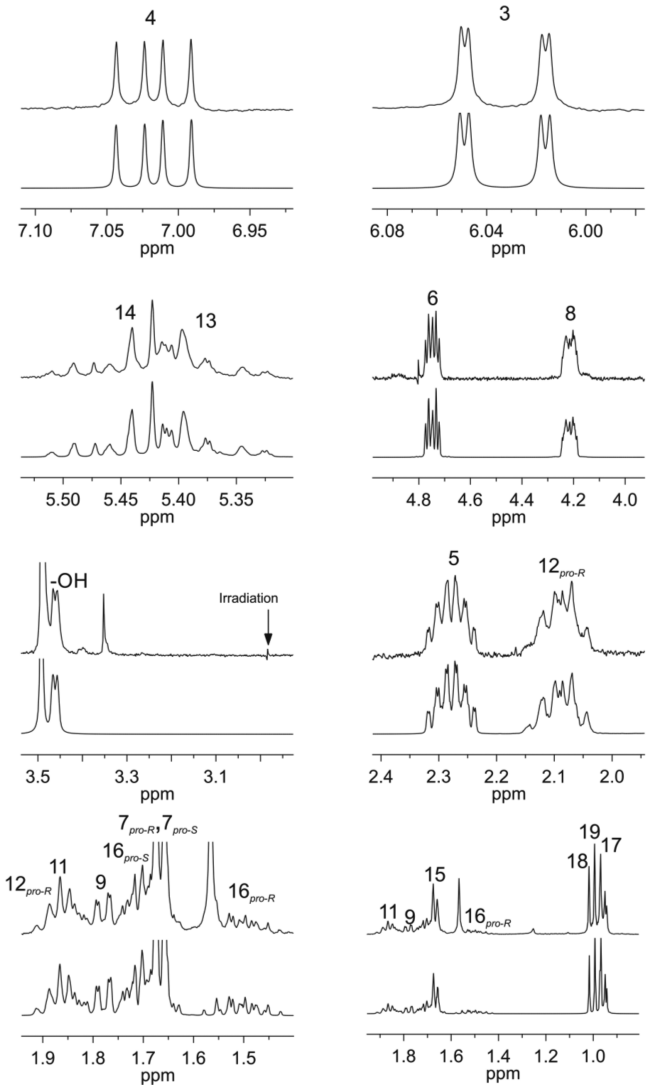

Figure 4. Comparison between the experimental ^1H NMR spectrum of pironetin in $CDCl_3$ at 300 MHz measured under irradiation of H-10 (upper traces) and the simulated spectrum (lower traces) obtained with RMS of 0.41 Hz. Assignments were confirmed by 2D NMR.

Pironetin−tubulin Interactions. Docking studies[25] can determine the optimum conformation and binding mode of pironetin to α-tubulin to inhibit the polymerization process and provide a quantitative model that includes the atomic coordinates and energy for the resulting entire system. This model can also be followed through a time−course study using molecular dynamics (MD)[26] and used as a valuable tool for characterizing protein−ligand sequences and their interactions in solution. Since pironetin covalently binds to tubulin at αLys352, a binding model was also generated in order to explore the protein conformational changes when the ligand is attached to tubulin. Visualization and evaluation of these models could eventually be useful in the design of more

dx.doi.org/10.1021/jo500420j | J. Org. Chem. 2014, 79, 3752−3764

Table 4. Detailed ^{1}H NMR Assignments of Pironetin[a]

H	δ (integral, multiplicity, J (Hz))
3	6.0284 (1H, ddd, $J_{3,4}$ = 9.8, $J_{3,5}$ = −1.1, $J_{3,16proS}$ = 0.2)
4	7.0132 (1H, dddd, $J_{3,4}$ = 9.8, $J_{4,5}$ = 6.0, $J_{4,6}$ = −0.1, $J_{4,16proS}$ = −0.3)
5	2.2865 (1H, ddddddd, $J_{3,5}$ = −1.1, $J_{4,5}$ = 6.0, $J_{5,6}$ = 3.5, $J_{5,7proR}$ = −0.2, $J_{5,7proS}$ = 0.5, $J_{5,8}$ = 0.5, $J_{5,16proR}$ = 9.7, $J_{5,16proS}$ = 4.7)
6	4.7404 (1H, ddddddd, $J_{4,6}$ = −0.1, $J_{5,6}$ = 3.5, $J_{6,7proR}$ = 2.5, $J_{6,7proS}$ = 9.9, $J_{6,8}$ = 0.4, $J_{6,16proR}$ = −0.7, $J_{6,16proS}$ = −0.5)
7*proR*	1.7270 (1H, ddddddd, $J_{5,7proR}$ = −0.2, $J_{6,7proR}$ = 2.5, $J_{7proR,7proS}$ = −13.7, $J_{7proR,8}$ = 9.7, $J_{7proR,9}$ = −0.5, $J_{7proR,16proR}$ = 0.2, $J_{7proR,16proS}$ = 0.7, $J_{7proR,OH}$ = −1.2)
7*proS*	1.6845 (1H, ddddddd, $J_{5,7proS}$ = 0.5, $J_{6,7proS}$ = 9.9, $J_{7proR,7proS}$ = −13.7, $J_{7proS,8}$ = 2.7, $J_{7proS,9}$ = −0.2, $J_{7proS,16proR}$ = 0.2, $J_{7proS,OH}$ = −0.5)
8	4.2053 (1H, ddddddd, $J_{5,8}$ = 0.5, $J_{6,8}$ = 0.4, $J_{7proR,8}$ = 9.7, $J_{7proS,8}$ = 2.7, $J_{8,9}$ = 1.7, $J_{8,11}$ = 0.4, $J_{8,18}$ = 0.4, $J_{8,OH}$ = 3.0)
9	1.7820 (1H, ddddddd, $J_{7proR,9}$ = −0.5, $J_{7proS,9}$ = −0.2, $J_{8,9}$ = 1.7, $J_{9,10}$ = 4.0, $J_{9,11}$ = −0.5, $J_{9,12proS}$ = 0.5, $J_{9,18}$ = 7.1, $J_{9,OH}$ = −0.3)
10	2.9835 (1H, dd, $J_{9,10}$ = 4.0, $J_{10,11}$ = 6.6)
11	1.8586 (1H, ddddddddd, $J_{8,11}$ = 0.4, $J_{9,11}$ = −0.5, $J_{10,11}$ = 6.6, $J_{11,12proR}$ = 8.0, $J_{11,12proS}$ = 4.3, $J_{11,13}$ = −0.2, $J_{11,14}$ = −0.4, $J_{11,18}$ = −0.4, $J_{11,19}$ = 6.9)
12*proR*	1.8650 (1H, ddddd, $J_{11,12proR}$ = 8.0, $J_{12proR,12proS}$ = −13.5, $J_{12proR,13}$ = 7.3, $J_{12proR,14}$ = −1.4, $J_{12proR,15}$ = 1.1)
12*proS*	2.0980 (1H, ddddddd, $J_{9,12proS}$ = 0.5, $J_{11,12proS}$ = 4.3, $J_{12proR,12proS}$ = −13.5, $J_{12proS,13}$ = 6.4, $J_{12proS,14}$ = −1.1, $J_{12proS,15}$ = 1.3, $J_{12proS,19}$ = 0.3)
13	5.3735 (1H, ddddd, $J_{11,13}$ = −0.2, $J_{12proR,13}$ = 7.3, $J_{12proS,13}$ = 6.4, $J_{13,14}$ = 14.8, $J_{13,15}$ = −1.5, $J_{13,19}$ = 0.2)
14	5.4422 (1H, ddddd, $J_{11,14}$ = −0.4, $J_{12proR,14}$ = −1.4, $J_{12proS,14}$ = −1.1, $J_{13,14}$ = 14.8, $J_{14,15}$ = 6.3)
15	1.6685 (3H, dddd, $J_{12proR,15}$ = 1.1, $J_{12proS,15}$ = 1.3, $J_{13,15}$ = −1.5, $J_{14,15}$ = 6.3)
16*proR*	1.5065 (1H, dddddd, $J_{5,16proR}$ = 9.7, $J_{6,16proR}$ = −0.7, $J_{7proR,16proR}$ = 0.2, $J_{7proS,16proR}$ = 0.2, $J_{16proR,16proS}$ = −13.6, $J_{16proR,17}$ = 7.5)
16*proS*	1.6985 (1H, dddddd, $J_{3,16proS}$ = 0.2, $J_{4,16proS}$ = −0.3, $J_{5,16proS}$ = 4.7, $J_{6,16proS}$ = −0.5, $J_{7proR,16proS}$ = 0.7, $J_{16proR,16proS}$ = −13.6, $J_{16proS,17}$ = 7.5)
17	0.9693 (3H, dd, $J_{16proR,17}$ =7.5, $J_{16proS,17}$ = 7.5)
18	1.0063 (3H, ddd, $J_{8,18}$ = 0.4, $J_{9,18}$ = 7.1, $J_{11,18}$ = −0.4)
19	0.9620 (3H, ddd, $J_{11,19}$ = 6.9, $J_{13,19}$ = 0.2, $J_{12proS,19}$ = 0.3)
OH	3.4398 (1H, dddd, $J_{7proR,OH}$ = −1.2, $J_{7proS,OH}$ = −0.5, $J_{8,OH}$ = 3.0, $J_{9,OH}$ = −0.3)
OMe	3.4742 (3H, s)

[a]Experimental spectrum measured in $CDCl_3$ at 300 MHz. Chemical shifts are in ppm and coupling constants in hertz. Data were obtained by nonlinear fit of the experimental ^{1}H NMR spectrum to the simulated spectrum with RMS = 0.37 Hz.

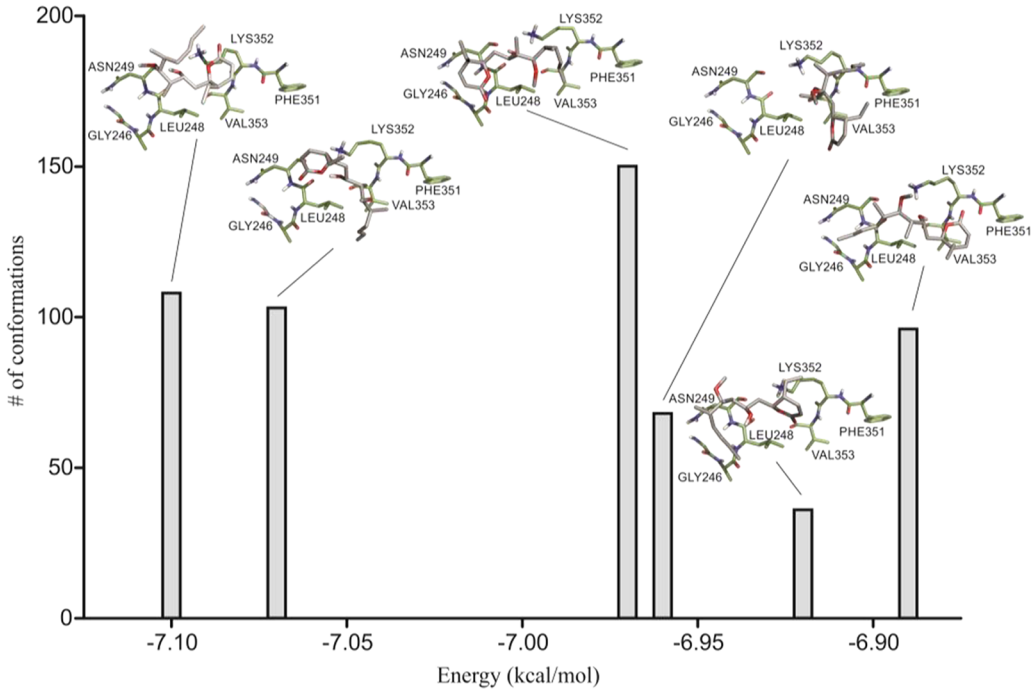

Figure 5. Clustering histogram for the six high-scoring pironetin−tubulin complexes.

selective tubulin interacting compounds based on this polyketide.

Docking Study. There are several X-ray structural studies available from the RCSB Protein Data Bank containing crystallographic coordinates for tubulin. Some studies provide the coordinates for the α,β-tubulin heterodimer as the basic structural unit of microtubules,[27,28] while others offer the coordinates for $\alpha,\beta,\alpha,\beta$-tetrameric complexes,[29] which in some cases included associated proteins for stabilizing the macrostructures. In the present study, the tubulin atomic coordinates were obtained from the 1JFF crystallographic file, which corresponds to *Bos taurus* α,β-tubulin heterodimer cocrystallized with paclitaxel, GDP, GTP, Zn^{2+}, and Mg^{2+} refined at 3.50 Å resolution.[27] We consider this file as the most appropriate for our purposes dedicated to model the interaction between such heterodimer and pironetin as an inhibitor of the protein polymerization. The more elaborated tetrameric complexes, designed to explain microtubule stability, were not evaluated in this study. The pironetin minimum energy molecular model (**1**-1) described above was utilized as the starting point for the

dx.doi.org/10.1021/jo500420j | J. Org. Chem. 2014, 79, 3752−3764

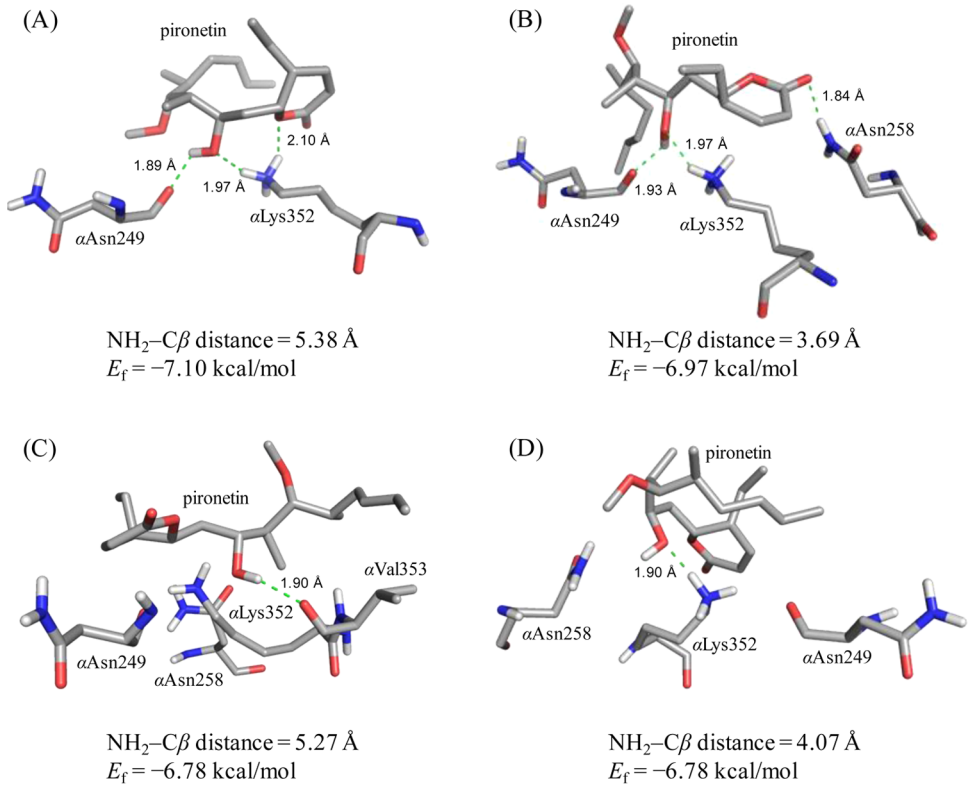

Figure 6. Highest scoring complexes between pironetin and tubulin originated from the *L*-type conformer **1**-1 (A and B) and from the *M*-type conformer **1**-13 (C and D). The distance between the αLys352 amino group and the β carbon atom of the α,β-unsaturated lactone (NH_2–Cβ), the docking energy (E_f), and the hydrogen bond distances are indicated.

ligand preparation. Default values were assigned for the ligand torsion[30] tree and for the Gasteiger–Marsili charges[31] by means of the AutoDock Tools program. A preliminary scanning on the protein surface was carried out using the AutoDock Vina program[32] and then the AutoDock 4 program[33] for a refined simulation of 1000 complexes. Specific features of interaction between pironetin and tubulin were taken into account for the scoring process. They were (a) the distance between the αLys352 amino group and the β carbon atom of the α,β-unsaturated lactone, (b) the number of hydrogen bonds, (c) the docking energy of complexes, and (d) the number of hydrophobic contacts. Figure 5 shows the six most representative binding modes of pironetin clustered according to their conformation and docking energy. In all these cases, pironetin remained close to the surface behind the αLys352 residue, displaying high-affinity for this protein site.

The most stable complex (Figure 6A) was found at E_f = −7.10 kcal/mol and showed hydrogen bond interactions between the hydroxyl group at C-8 of pironetin and the peptide carbonyl group of αAsn249 (1.89 Å). Interactions among the αLys352 amino group hydrogen atoms and both O-1 and O-8 of pironetin (2.10 and 1.97 Å, respectively) were also observed. The most frequently found complex orientation (Figure 6B) was at E_f = −6.97 kcal/mol and showed hydrogen bond interactions between the carbonyl group at C-2 of pironetin with one amide hydrogen of αAsn258 (1.84 Å). The hydroxyl group at C-8 in pironetin also interacted with the peptide carbonyl group of αAsn249 (1.93 Å) and with the αLys352 amino group hydrogen atoms (1.97 Å). Both complexes were located at the entrance of the small pocket found between the α-helix H8, β-sheet S9 and α-helix H10 (Figure 7) near the surface behind αLys352, agreeing with the

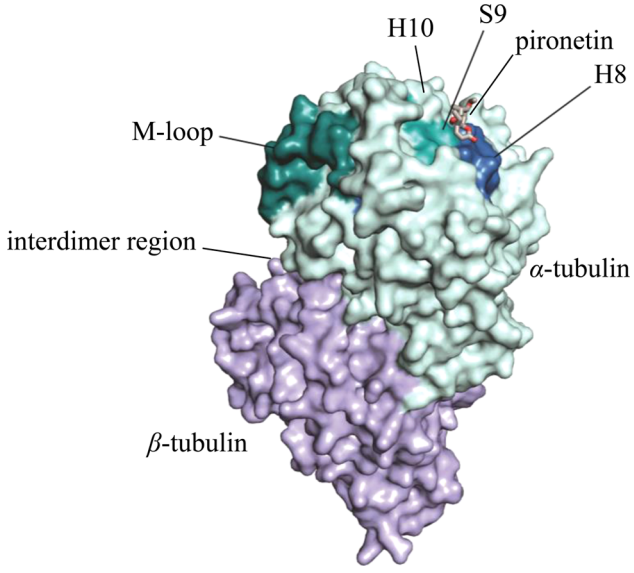

Figure 7. Structure of the most frequent pironetin–tubilin complex (E_f= −6.97 kcal/mol), showing the interdimer surface region, the H8 and H10 α-helices, the S9 β-sheet, and the M-loop. The internuclear distance between the αLys352 amino group and the β-carbon atom of the α,β-unsaturated lactone ring is 3.69 Å.

binding site proposed by Usui et al.[5] In both situations, the distance between the αLys352 amino group and the β carbon atom of the α,β-unsaturated lactone ring was close enough to favor a Michael addition: 3.69 Å for the most frequent and 5.38 Å for the most stable complexes. Other conformational arrangements at this binding site were detected in the full

dx.doi.org/10.1021/jo500420j | J. Org. Chem. 2014, 79, 3752–3764

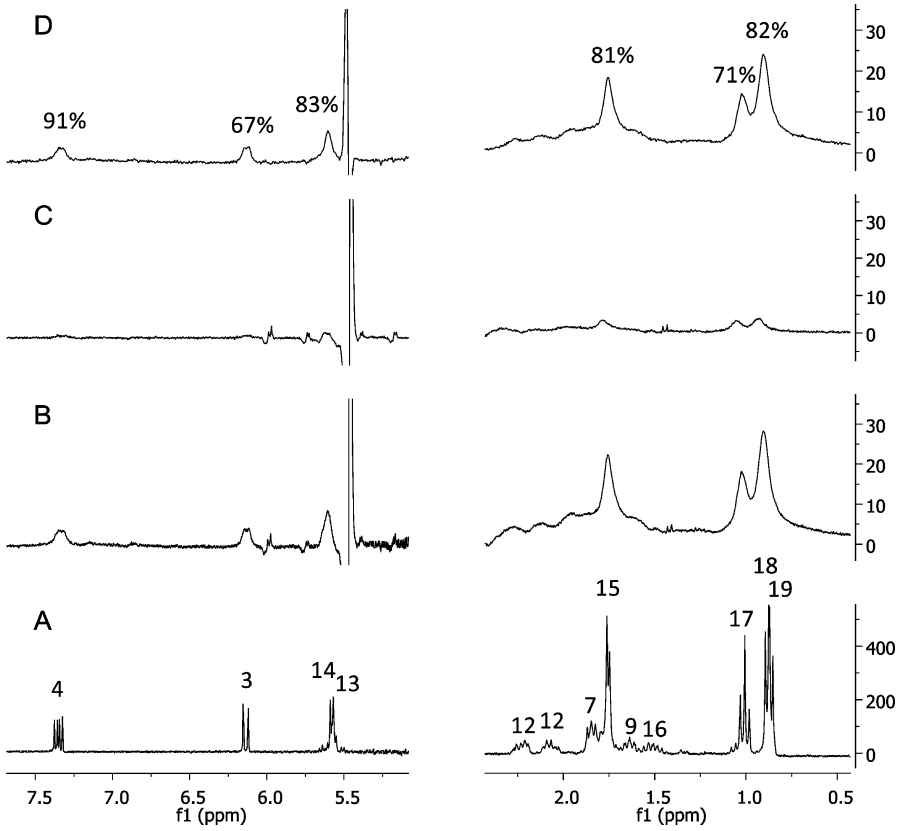

Figure 8. STD NMR spectra showing the vinylic and aliphatic regions. (A) Spectrum of 2 mM pironetin measured in 10 mM sodium phosphate buffer pD 7.2 in 99.9% D_2O with DMSO-d_6 (5% v/v) at 25 °C. (B) *Off-resonance* spectrum of pironetin obtained in the presence of 20 μM α,β-tubulin and 5 mM sucrose under irradiation at −9 ppm. (C) *On-resonance* spectrum of the pironetin−tubulin complex obtained under irradiation at 0 ppm. (D) Corresponding difference spectrum including saturation transfer effects.

clustering histogram of the pironetin-tubulin interaction (Figure S2, Supporting Information). However, they exhibited higher docking energies and less favorable scoring results compared to the complexes depicted in Figures 6A and 6B. A second docking procedure was performed using the *M*-type conformer **1**-13, as the initial ligand geometry, and by releasing all the rotatable bonds. Several additional low energy complexes were obtained but they had either longer distances between the αLys352 amino group and the β carbon atom of the α,β-unsaturated lactone or a smaller number of hydrogen bonds. Two representative complexes of this second process are depicted in Figure 6C,D. Since *M*-type conformers are preferred in polar solvents, it is conceivable that they can be involved in the first stages of the ligand approach. After that, the protein surface may alter the medium lipophilicity and consequently may change the conformation and binding mode. The most important feature for a highly favorable complex is the presence of a short distance between the αLys352 amino group and the β carbon atom of the α,β-unsaturated lactone, as in the complex of Figure 6B. This proximity favors the covalent binding to αLys352 that ultimately shifts the equilibrium toward an irreversible adduct formation.

Additionally, the complex of Figure 6B displayed hydrophobic interactions between the C-15 methyl group and one terminal methyl group of αLeu248 with a distance of 3.52 Å and between C-15 and the methine group of αVal353 with a distance of 3.97 Å, while the β carbon atom of the α,β-unsaturated lactone showed interaction with the β carbon atom of αAsn249 with a distance of 3.81 Å, positioning this arrangement as the one with the highest scoring.

Saturation-transfer difference (STD) NMR spectroscopy[34,35] was used to complement the docking study with experimental data in order to demonstrate the pironetin−tubulin interactions. Figure 8 shows the vinylic and aliphatic regions of the STD NMR spectra of pironetin, which were measured using sodium phosphate buffer in D_2O with 5% DMSO-d_6 in the presence of α,β-tubulin and sucrose at 25 °C. Under these conditions, all signals could be measured with the exception of those for H-6, H-8, and H-10, which were difficult to evaluate due to their overlapping with HDO and sucrose signals. Figure 8A shows the spectrum of pironetin without the protein, while Figure 8B shows the *off-resonance* spectrum of pironetin in the presence of tubulin in a 100:1 molar ratio. The protein induced a notable broadening of the pironetin signals, as a consequence of protein binding.[35] The line widths changed from 1 to 2 Hz in the ligand spectrum alone to 16−24 Hz in the spectrum of the complex. This change was not observed in the sucrose signals, which remained with line widths of 1−2 Hz. Figure 8C shows the *on-resonance* spectrum where strong signal saturation occurred, and Figure 8D shows the difference spectrum indicating a marked interaction between the ligand and the protein. Saturation transfer values were in agreement with the pironetin−tubulin complexes depicted in Figure 6A,B. The C-18 methyl group remained closer to the protein surface, while C-17, as part of the ethyl chain, pointed outward in some poses toward the opposite side yielding a slightly smaller STD effect. The functionality of the pironetin−tubulin complex employed

dx.doi.org/10.1021/jo500420j | J. Org. Chem. 2014, 79, 3752−3764

in this work was confirmed by polymerization inhibition assays based on optical density measurements. Tubulin polymerization was reduced by 77% with respect to the control after 60 min of interaction with pironetin (Figure S5, Supporting Information).

Molecular Dynamics. MD of pironetin−tubulin was carried out with the α,β-tubulin dimer which included water molecules, cofactors, and ions. This analysis was based on the protocol described by Shanker et al. for the paclitaxel−tubulin dynamic interaction,[26] using the GROMACS program[36] for the simulation, the GROMOS force field[37] for ligand parametrization, as well as the Berendsen[38] and Parrinello−Rahman[39] thermostats for protein parametrization as described in the Experimental Section. The most frequently found pironetin−tubulin complex (E_f = −6.97 kcal/mol) in the docking analysis was the starting point geometry for the molecular dynamics to which was incorporated one GDP molecule, one GTP molecule, two Mg^{2+} ions, 34 Na^+ ions, and approximately 40000 H_2O molecules. This protein−ligand complex was initially subjected to a position-restrained molecular dynamics run to accommodate the nucleoside phosphates, solvent molecules, and ions in adequate locations. MD at 20 K followed without position restraints in order to release the molecular tension generated by the crystallographic interactions and equilibrate the entire system to a starting point. The system was gradually heated to 300 K, and 3 ns MD simulations were performed as can be seen in video S1 (Supporting Information).

Since the probability of a covalent reaction between tubulin and pironetin is a function of the distance between the tubulin αLys352 Nε amino group and the pironetin C-β position of the α,β-unsaturated lactone, distances were monitored during the MD simulations. A representative plot is presented in Figure 9 together with the Coulomb potential variations of the distance between the two atoms.

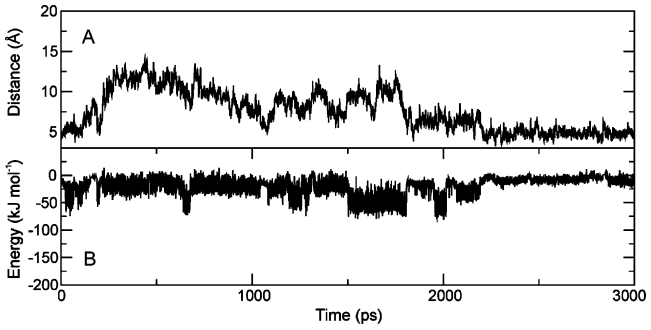

Figure 9. Time−course measurements for (A) the internuclear distance between the αLys352 Nε amino group and the β carbon atom of the α,β-unsaturated lactone ring and (B) the corresponding Coulomb potential.

Some cytotoxic compounds affect the molecular recognition and affinity between both tubulin α and β protein subunits, modifying their polymerization−depolymerization process.[1,2] In order to evaluate these conformational fluctuations, the cumulative root-mean-square deviations of tubulin atomic coordinates were measured during its interaction with pironetin and subtracted from those without the ligand. Figure 10 shows the ΔRMS for the tubulin atoms located in the M-loop of the α-subunit between αIle274 and αLeu285. It is known that the M-loop is essential for protofilament interaction during tubulin

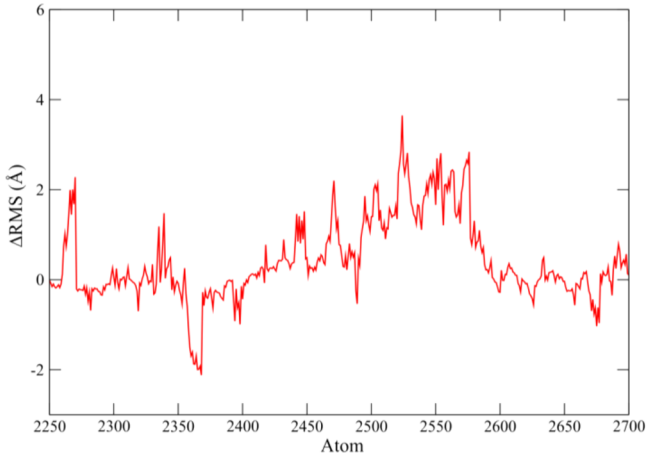

Figure 10. Cumulative root-mean-square deviations of the α-tubulin M-loop atomic coordinates during its interaction with pironetin. The RMS values were subtracted from those measured without the ligand to give ΔRMS.

polymerization,[27] and in this region the largest variations occurred during the molecular recognition of both laterally associated subunits.

Debye−Waller factors or *B*-factors[40] were calculated for the protein atoms during the 3000 ps molecular dynamics simulations at 300 K, estimating the conformational variations that took place during protein−ligand interaction. A notable variation was observed between tubulin without the ligand and tubulin complexed with pironetin. The color scale representation of Figure 11 shows the *B*-factor differences, particularly of the α-tubulin M-loop, oriented toward the center of the macromolecules. Tables with the atomic coordinates and B-factors are included in Tables S4 and S5 (Supporting Information).

Pironetin−Tubulin Covalent Adduct Molecular Modeling. The molecular modeling was carried out using the ONIOM approach[41] starting from the most frequently found pironetin−tubulin orientation (Figure 6B). In the covalent complex, the Nε atom of αLys352 was bonded to C-4 of pironetin in a Michael addition trajectory, resulting in a new chiral center at C-4 with an *S* configuration (Figure 12). This model was obtained after several steps, including (1) balancing the number of hydrogen atoms in the αLys352 and pyrone moieties, (2) inclusion of a net charge −16 for the tubulin α-subunit, (3) pre-refinement of the entire covalent complex by means of molecular mechanics with the UFF force field, (4) selection of a 6.5 Å zone surrounding the pironetin moiety centered at C-4, and (5) geometry optimization with the Hartree−Fock quantum method using the 3-21G basis set for the selected 6.5 Å zone and with the UFF force field for the remaining portion of the protein.

The resulting model showed the hydrogen-bond interaction between the carbonyl group at C-1 in pironetin and one hydrogen atom of the αAsn258 NH with an internuclear distance of 2.54 Å, observable since the docking model. A hydrogen-bond interaction was also found between the hydroxyl hydrogen at C-8 and the carboxyl group of αGlu254, having 2.33 Å as its interatomic distance. It is known that this residue, located in the proximity of the hydrolyzing γ-GTP of the tubulin β-unit, acts as a catalytic entity crucial to tubulin protofilament formation and is highly preserved in eukaryotic cells.[27] In addition to the hydrogen

dx.doi.org/10.1021/jo500420j | J. Org. Chem. 2014, 79, 3752−3764

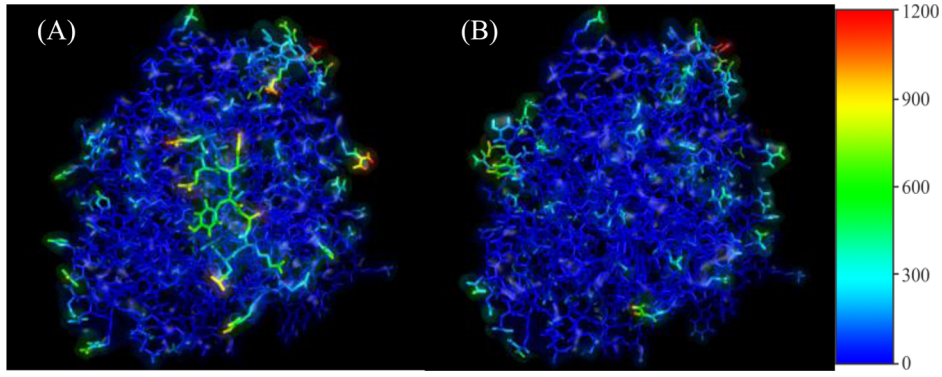

Figure 11. Debye–Waller factors or *B*-factors for (A) α-tubulin interacting with pironetin and (B) α-tubulin without the ligand. In both models, the M-loop was oriented toward the center of the image while pironetin in (A) is located in the rear of the protein. Fluctuations are indicated in the color scale bar in Å^2.

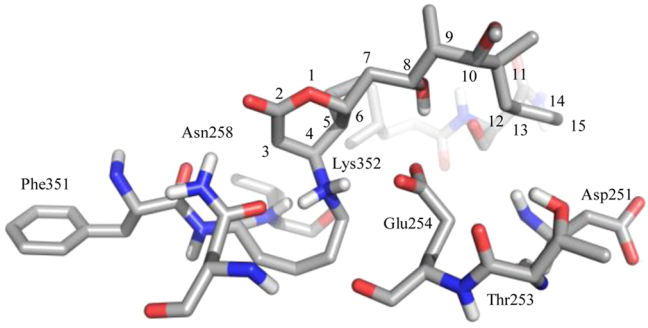

Figure 12. Region of the ONIOM model showing pironetin covalently bonded to αLys352 and its hydrogen-bond interactions with αGlu254 and αAsn258.

bond interactions, the model showed a close proximity between the pironetin ethyl group and the isobutyl residue of αLeu248 where the shortest distance between the two alkyl group hydrogens is ca. 2.50 Å.

Figure 13 shows the structural changes undergone by α-tubulin: (A) the crystallographic structure, (B) the minimized structure without the ligand, (C) the modeled tubulin structure with docked pironetin without the covalent bond, and (D) tubulin with pironetin covalently bonded through αLys352. A substantial variation was observed in the protein structure in the covalently bonded pironetin–tubulin complex (Figure 13D) as compared to the crystallographic file (Figure 13A), the minimized structure without the ligand (Figure 13B), and docked pironetin model (Figure 13C). The changes in the S9 β-sheet that contains αLys352 were notable, and α-helices H8

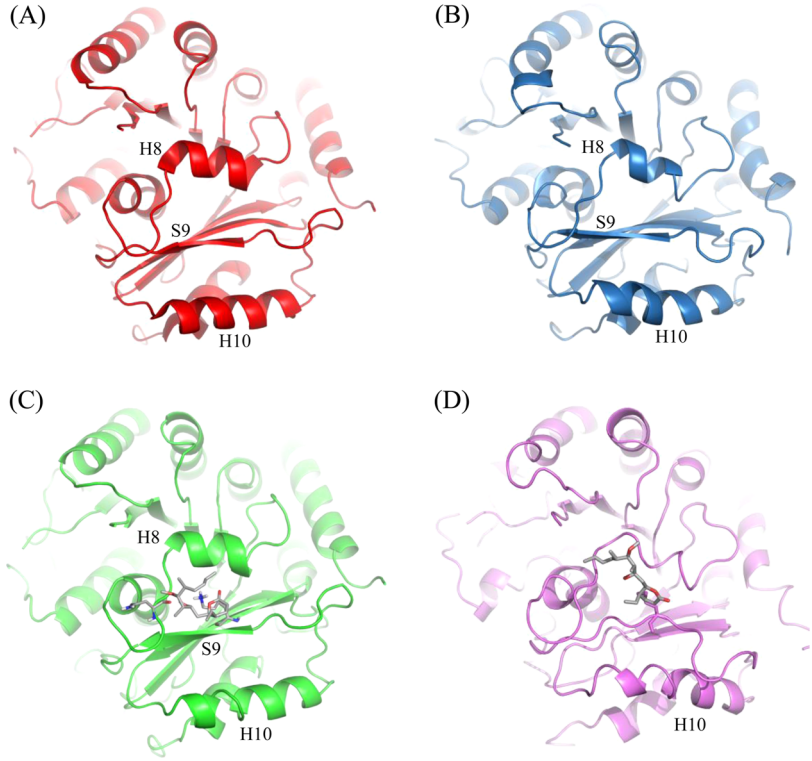

Figure 13. Structures of α-tubulin: (A) 1JFF crystallographic model, (B) minimized model without ligands, (C) protein model with docked pironetin, and (D) minimum energy molecular model with pironetin covalently bonded at αLys352.

dx.doi.org/10.1021/jo500420j | J. Org. Chem. 2014, 79, 3752–3764

and H10 showed significant variations in their secondary structures (Figure S3, Supporting Information). Results also indicated that the α-tubulin M-loop underwent a major conformational change when the protein interacted with pironetin (Figure 14 and Figure S4, Supporting Information),

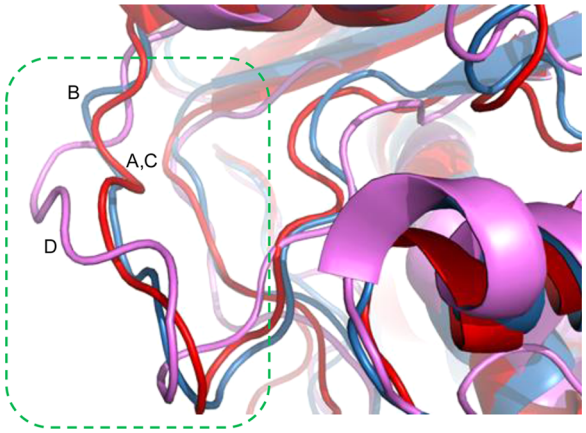

Figure 14. Superimposed M-loop structures of α-tubulin: (A) 1JFF crystallographic model, (B) minimized model without ligands, (C) minimized model with docked pironetin, and (D) minimum energy model with pironetin covalently bonded at αLys352.

reinforcing that the M-loop plays an essential role in the lateral contact between the $\alpha-\alpha$ y $\beta-\beta$ units of adjacent protofilaments and their structural modifications altered the molecular recognition during the polymerization of tubulin.[27]

CONCLUSION

Conformational studies of the anticancer agent pironetin, carried out by density functional theory calculations (B3PW91/DGTZVP) as well as by comparison of theoretical and experimental ^{1}H−^{1}H coupling constants, evidenced pironetin's extreme flexibility. A total of 53 conformational arrangements within the first 3 kcal/mol ΔG range were clustered in two conformational families depending on the surrounding media polarity, the *L*-type having an intramolecular hydrogen bond (prevalent in $CHCl_3$) and the *M*-type with an extended chain arrangement (prevalent in MeOH). These results offer a detailed and quantitative description for the conformational behavior of pironetin that is essential to be considered for the design of new pironetin-based bioactive compounds.

Docking studies, together with STD experiments, provided a quantitative model that reinforces the proposed mechanism of action for pironetin. The two most favorable binding modes found in the pironetin−tubulin complex showed a close distance between the αLys352 amino group and the β carbon atom of the α,β-unsaturated lactone which facilitates the formation of an irreversible covalent adduct. Molecular dynamics in water of the protein−ligand interaction as well as the minimized pironetin-tubulin covalent adduct molecular model both showed a major conformational perturbation at the M-loop in the α-tubulin subunit which plays a key role in molecular recognition between $\alpha-\alpha$ and $\beta-\beta$ units of protofilaments. Such a measurable variation is in agreement with the observed disruption of tubulin polymerization in the presence of pironetin.

EXPERIMENTAL SECTION

Nuclear Magnetic Resonance. Experimental ^{1}H NMR spectra of pironetin (Enzo Life Sciences) were measured at 300 MHz using tetramethylsilane as the internal standard. Spectral assignments were confirmed by COSY, *g*HSQC, and *g*HMBC spectra. ^{1}H−^{1}H NMR coupling constants were determined through spectral simulation, which was carried out in the MestReNova v 6.0.2.[24] Comparison between DFT-calculated and experimental coupling constants was estimated, taking into account the root-mean-square error (σ) according to the following equation:

$$\sigma = \left[\frac{1}{N}\sum_{i}^{N}(J_{\text{calc}} - J_{\text{exp}})^2\right]^{1/2}$$

Conformational Analysis and Coupling Constants Calculations. The conformational search for pironetin was carried out in the Spartan'04 for Windows program[14] by using the Monte Carlo method[15] and the MMFF94 molecular mechanics force field.[16] A total of 967 geometrically different structures were collected within an energy range between 0 and 15 kcal/mol. DFT single-point calculations were achieved at the B3LYP/6-31G(d) level of theory[17] giving 107 conformers in a ΔE = 0.0−4.5 kcal/mol range. All these structures were DFT optimized in the Gaussian 03 program[19] at the B3PW91/DGTZVP level of theory on a GNU/Linux operating system loaded in a cluster, which includes 1368 processors at 2.6 GHz and a RAM memory of 3 terabytes. For each job, a maximum of four processors was used. After optimization, the vibrational frequencies were calculated to obtain ΔG values, yielding 53 conformers within a ΔG range of 0.0−3.0 kcal/mol. The conformers were confirmed as true minima by the lack of imaginary vibrational frequencies. The Boltzmann populations for all conformers were calculated with the equation

$$P_i = \frac{e^{-\Delta G_i/k_B T}}{\sum_{i=1}^{n} e^{-\Delta G_i/k_B T}}$$

where P_i is the Boltzmann population for the *i*th conformer; ΔG_i is the Gibbs free energy for the *i*th conformer relative to the global minimum; k_B is the Boltzmann constant (0.0019872 kcal/(mol K)); and T is temperature (K) (298 K). Magnetic shielding tensors were calculated with the GIAO method, and the coupling constants were calculated as the sum of the Fermi contact, diamagnetic spin−orbit, spin−dipolar, and paramagnetic spin−orbit obtained from the B3PW91/DGTZVP optimized structures by using the *spinspin* option in the Gaussian 03 program.[19]

Docking Study. The AutoDock Tools 1.5.4 package (The Scripps Research Institute, La Jolla, CA) was employed for addition of polar hydrogen atoms, Gasteiger-Marsili charges, and solvation parameters to the 1JFF.PDF structure of α,β-tubulin which was combined with the molecular model of pironetin. The entire system was subjected to a preliminary surface scanning with AutoDock Vina 1.0 for GNU/Linux[32] followed by a refined docking with AutoDock 4.2[33] program, considering the αLys352 residue as flexible and a grid box size set at 40 Å × 40 Å × 40 Å in the *x*, *y*, and *z* dimensions centered at the nitrogen atom of the αLys352 residue. Docking calculations were carried out in computers operating at 3.2 GHz with 8 Gb RAM in the GNU/Linux environment.

Saturation-Transfer Difference Experiments. A solution containing 20 μM α,β-tubulin, 2 mM pironetin, 5 mM sucrose, and 10 mM sodium phosphate buffer pD 7.2 in 99.9% D_2O with DMSO-d_6 (5% v/v) was equilibrated during at least 30 min at 25 °C before measuring the NMR spectra. STD-NMR experiments were acquired at 298.1 K with 512 transients in a matrix with 64 K data points and a spectral window of 10000 Hz. The spectra were recorded at 300 MHz by irradiating at 0 ppm during the *on-resonance* and at −9 ppm for the *off-resonance* experiments. Protein saturation was carried out using 50 ms Gauss-shaped pulses for a total saturation time of 2.0 s. Control spectra were recorded under identical conditions on samples containing pironetin or tubulin. The *on-resonance* and *off-resonance*

dx.doi.org/10.1021/jo500420j | J. Org. Chem. 2014, 79, 3752−3764

spectra were processed independently and subtracted to provide the differential spectrum.

Inhibition of Tubulin Polymerization. The influence of pironetin in tubulin polymerization was evaluated by optical density measurements since this property is proportional to microtubule formation. Freshly reconstituted solutions (100 μL) of 2 mg/mL tubulin >99% (Cytoskeleton, Inc.) in tubulin buffer [80 mM piperazine-*N*,*N*′-bis(2-ethanesulfonic acid) sodium salt, 0.5 mM ethylene glycol−bis(β-aminoethyl ether)−*N*,*N*,*N*′,*N*′-tetraacetic acid, and 2 mM $MgCl_2$ at pH 7.0] and 1 mM guanosine-5′-triphosphate were combined at 4 °C with 10 μM pironetin solutions (10 μL) in DMSO using a half area 96-well plate. The mixtures were incubated at 37 °C under stirring in an absorbance microplate reader. Protein polymerization was monitored by measuring absorbance every minute during 60 min at 340 nm. The reading at time zero was subtracted from subsequent readings to obtain Δ absorbance. Assays were carried out in triplicate, and graphs were prepared in GraphPad Prism (GraphPad Software). The results were evaluated using an analysis of variance followed by a Tukey's test, $P < 0.05$.

Molecular Dynamics. The crystallographic structure of α,β-tubulin, containing two Mg^{2+} atoms, was converted to the GROMOS 96.1 (ffG43a1) force field.[42] Geometries for GDP and GTP were optimized in the Spartan'04 program at the DFT/B3LYP/6-31G level of theory and further parametrized for GROMOS 96.1 in the PRODRG server.[42] The parametrized complex including α,β-tubulin, two Mg^{2+} atoms, one GDP, and one GTP was neutralized with 34 Na^+ atoms and placed into a cubic arrangement with 39313 H_2O molecules according to the single-point charge model.[43] Molecular dynamics simulations were performed with the GROMACS 4.0.3 program[36] compiled for the LAM-OpenMPICH parallel run-time environment (The Ohio Supercomputer Center at The Ohio State University, University of Notre Dame, and the Pervasive Technology Laboratories at Indiana University) using three nodes of Core 2 Duo processors operating at 3 GHz with 8 Gb RAM in a 64-bit GNU Linux system. The entire molecular complex was subjected to a steepest descent minimization procedure[26] followed by a 40 ps protein−ligand restrained MD simulation for allowing H_2O molecules, GDP, GTP, and ions to equilibrate around the protein structure under isothermal conditions by using the Berendsen thermostat.[38] The system was first subjected to a MD simulation without restrictions at 50 K for 15 ps, in order to alleviate high energy interactions, and then heated gradually from 20 to 300 K over a period of 30 ps. The complex was subjected to five independent MD simulations for 5 ns each, using the Particle Mesh Ewald electrostatics method[44] with a 0.9 nm cutoff. MD calculations were performed under NPT conditions employing the Nosé−Hoover thermostat,[45,46] the Parrinello−Rahman barostat,[39] and a time step of 1 fs. Data analysis, trajectory visualization, and distance measurements were accomplished with the VMD 1.8.6 program.[47]

Molecular Modeling of the Pironetin−Tubulin Covalent Adduct. The most frequent pose for the pironetin−tubulin complex was loaded into the GaussView 05 program to form the covalent bond between the Nε atom of αLys352 and C-4. In this same program, the hydrogen atoms and the net charge for the protein −16 were adjusted. Energy minimizations and refinements were performed in the Gaussian 09 program[48] employing the ONIOM (HF/3-21G:UFF) method.[41]

■ ASSOCIATED CONTENT

Ⓢ Supporting Information

Experimental and simulated ^1H NMR, ^{13}C NMR, COSY, NOESY, HSQC, and HMBC spectra of pironetin. Conformational clustering histogram for the pironetin−tubulin complexes. DFT relative free energies, population, as well as theoretical and experimental $^1H-^1H$ coupling constants of pironetin. Cartesian coordinates for the global minimum energy structure of pironetin. Coordinates and simulated *B*-factors for the M-loop of α-tubulin with and without pironetin. Superimposed structures and RMSD values of α-tubulin models and those for the M-loop. A video showing the molecular dynamics of pironetin−tubulin interaction. This material is available free of charge via the Internet at http://pubs.acs.org.

■ AUTHOR INFORMATION

Corresponding Author

*E-mail: ccerda@cinvestav.mx. Tel: +52 55 5747-4035. Fax: +52 55 5747-7137.

Notes

The authors declare no competing financial interest.

Taken in part from the Ph.D. Thesis of A. E. Bañuelos-Hernández presented to Posgrado del Departamento de Farmacología, Cinvestav.

■ ACKNOWLEDGMENTS

Financial support (Grant No. 104887) from Consejo Nacional de Ciencia y Tecnología (Mexico) and from Dirección General de Asuntos del Personal Académico, UNAM (IN212813) is acknowledged. A.E.B.-H. received a fellowship from CONACyT (Grant No. 207010). Geometry optimizations were performed in the HP Cluster Platform 4000 (KanBalam) at the Departamento de Supercómputo, Dirección General de Servicios de Cómputo Académico, Universidad Nacional Autónoma de México. We are grateful to Q.F.B. Yolanda Mora-Pérez (Departamento de Química, Cinvestav) for her valuable assistance in the STD experiments.

■ REFERENCES

(1) (a) Kingston, D. G. I. *J. Nat. Prod.* **2009**, *72*, 507−515. (b) Mollinedo, F.; Gajate, C. *Apoptosis* **2003**, *8*, 413−450.

(2) (a) Jiménez-Barbero, J.; Amat-Guerri, F.; Snyder, J. P. *Curr. Med. Chem.: Anti-Cancer Agents* **2002**, *2*, 91−122. (b) Canales, A.; Matesanz, R.; Gardner, N. M.; Andreu, J. M.; Paterson, I.; Díaz, J. F.; Jiménez-Barbero, J. *Chem.—Eur. J.* **2008**, *14*, 7557−7569. (c) Field, J. J.; Díaz, J. F.; Miller, J. H. *Chem. Biol.* **2013**, *20*, 301−315.

(3) Kondoh, M.; Usui, T.; Kobayashi, S.; Tsuchiya, K.; Nishikawa, K.; Nishikiori, T.; Mayumi, T.; Osada, H. *Cancer Lett.* **1998**, *126*, 29−32.

(4) Kondoh, M.; Usui, T.; Nishikiori, T.; Mayumi, T.; Osada, H. *Biochem. J.* **1999**, *340*, 411−416.

(5) Usui, T.; Watanabe, H.; Nakayama, H.; Tada, Y.; Kanoh, N.; Kondoh, M.; Asao, T.; Takio, K.; Watanabe, H.; Nishikawa, K.; Kitahara, T.; Osada, H. *Chem. Biol.* **2004**, *11*, 799−806.

(6) Kobayashi, S.; Tsuchiya, K.; Kurokawa, T.; Nakagawa, T.; Shimada, N.; Iitaka, Y. *J. Antibiot.* **1994**, *47*, 703−707.

(7) (a) Pereda-Miranda, R.; Hernández, L.; Villavicencio, M. J.; Novelo, M.; Ibarra, P.; Chai, H.; Pezzuto, J. M. *J. Nat. Prod.* **1993**, *56*, 583−593. (b) Collet, L. A.; Davies-Coleman, M. T. Rivett, D. E. A. Naturally occurring 6-substituted 5,6-dihydro-α-pyrones. In *Progress in the Chemistry of Organic Natural Products*; Herz, W., Falk, H., Kirby, G. W., Moore, R. E., Tamm, Ch., Eds.; Springer: New York, 1998; Vol. 75, pp 182−209. (c) Pereda-Miranda, R. Bioactive Natural Products from Traditionally Used Mexican Plants. In *Phytochemistry of Medicinal Plants*; Arnason, J. T., Mata, R., Romeo, J. T., Eds.; Plenum: New York, 1995; pp 83−112. (d) Pereda-Miranda, R.; Fragoso-Serrano, M.; Cerda-García-Rojas, C. M. *Tetrahedron* **2001**, *57*, 47−53. (e) Fragoso-Serrano, M.; Gibbons, S.; Pereda-Miranda, R. *Planta Med.* **2005**, *71*, 278−280. (f) Falomir, E.; Murga, J.; Ruiz, P.; Carda, M.; Marco, J. A.; Pereda-Miranda, R.; Fragoso-Serrano, M.; Cerda-García-Rojas, C. M. *J. Org. Chem.* **2003**, *68*, 5672−5676.

(8) (a) Dias, L. C.; de Oliveira, L. G.; de Sousa, M. A. *Org. Lett.* **2003**, *5*, 265−268. (b) Shen, X.; Wasmuth, A. S.; Zhao, J.; Zhu, C.; Nelson, S. G. *J. Am. Chem. Soc.* **2006**, *128*, 7438−7439. (c) Enders, D.; Dhulut, S.; Steinbusch, D.; Herrbach, A. *Chem.—Eur. J.* **2007**, *13*, 3942−3949. (d) Crimmins, M. T.; Dechert, A. M. R. *Org. Lett.* **2009**, *11*, 1635−1638. (e) Yadav, J. S.; Ather, H.; Rao, N. V.; Reddy, M. S.; Prasad, A. R. *Synlett* **2010**, 1205−1208.

(9) Yoshida, M.; Matsui, Y.; Ikarashi, Y.; Usui, T.; Osada, H.; Wakasugi, H. *Anticancer Res.* **2007**, *27*, 729−736.
(10) Vogt, A.; McPherson, P. A.; Shen, X.; Balachandran, R.; Zhu, G.; Raccor, B. S.; Nelson, S. G.; Tsang, M.; Day, B. W. *Chem. Biol. Drug Des.* **2009**, *74*, 358−368.
(11) Tamura, Y.; Simizu, S.; Muroi, M.; Takagi, S.; Kawatani, M.; Watanabe, N.; Osada, H. *Oncogene* **2009**, *28*, 107−116.
(12) (a) Carda, M.; Murga, J.; Díaz-Oltra, S.; García-Pla, J.; Paños, J.; Falomir, E.; Trigili, C.; Díaz, J. F.; Barasoain, I.; Marco, J. A. *Eur. J. Org. Chem.* **2013**, 1116−1123. (b) Paños, J.; Díaz-Oltra, S.; Sánchez-Peris, M.; García-Pla, J.; Murga, J.; Falomir, E.; Carda, M.; Redondo-Horcajo, M.; Díaz, J. F.; Barasoain, I.; Marco, J. A. *Org. Biomol. Chem.* **2013**, *11*, 5809−5826. (c) Marco, J. A.; García-Pla, J.; Carda, M.; Murga, J.; Falomir, E.; Trigili, C.; Notararigo, S.; Díaz, J. F.; Barasoain, I. *Eur. J. Med. Chem.* **2011**, *46*, 1630−1637.
(13) Torijano-Gutiérrez, S.; Vilanova, C.; Díaz-Oltra, S.; Murga, J.; Falomir, E.; Carda, M.; Marco, J. A. *Eur. J. Org. Chem.* **2014**, 2284−2296.
(14) Kong, J.; White, C. A.; Krylov, A. I.; Sherrill, D.; Adamson, R. D.; Furlani, T. R.; Lee, M. S.; Lee, A. M.; Gwaltney, S. R.; Adams, T. R.; Ochsenfeld, C.; Gilbert, A. T. B.; Kedziora, G. S.; Rassolov, V. A.; Maurice, D. R.; Nair, N.; Shao, Y.; Besley, N. A.; Maslen, P. E.; Dombroski, J. P.; Daschel, H.; Zhang, W.; Korambath, P. P.; Baker, J.; Byrd, E. F. C.; Van Voorhis, T.; Oumi, M.; Hirata, S.; Hsu, C.-P.; Ishikawa, N.; Florian, J.; Warshel, A.; Johnson, B. G.; Gill, P. M. W.; Head-Gordon, M.; Pople, J. A. *J. Comput. Chem.* **2000**, *21*, 1532−1548.
(15) Chang, G.; Guida, W. C.; Still, W. C. *J. Am. Chem. Soc.* **1989**, *111*, 4379−4386.
(16) (a) Halgren, T. *J. Comput. Chem.* **1996**, *17*, 490−519. (b) Halgren, T. *J. Comput. Chem.* **1996**, *17*, 520−552. (c) Halgren, T. *J. Comput. Chem.* **1996**, *17*, 553−586. (d) Halgren, T.; Nachbar, R. B. *J. Comput. Chem.* **1996**, *17*, 587−615. (e) Halgren, T. *J. Comput. Chem.* **1996**, *17*, 616−641.
(17) Francl, M. M.; Pietro, W. J.; Hehre, W. J.; Binkley, J. S.; DeFrees, D. J.; Pople, J. A.; Gordon, M. S. *J. Chem. Phys.* **1982**, *77*, 3654−3665.
(18) (a) Godbout, N.; Salahub, D. R.; Andzelm, J.; Wimmer, E. *Can. J. Chem.* **1992**, *70*, 560−571. (b) Andzelm, J.; Wimmer, E. *J. Chem. Phys.* **1992**, *96*, 1280−1303.
(19) Frisch, M. J.; Trucks, G. W.; Schlegel, H. B.; Scuseria, G. E.; Robb, M. A.; Cheeseman, J. R.; Montgomery, J. A., Jr.; Vreven, T.; Kudin, K. N.; Burant, J. C.; Millam, J. M.; Iyengar, S. S.; Tomasi, J.; Barone, V.; Mennucci, B.; Cossi, M.; Scalmani, G.; Rega, N.; Petersson, G. A.; Nakatsuji, H.; Hada, M.; Ehara, M.; Toyota, K.; Fukuda, R.; Hasegawa, J.; Ishida, M.; Nakajima, T.; Honda, Y.; Kitao, O.; Nakai, H.; Klene, M.; Li, X.; Knox, J. E.; Hratchian, H. P.; Cross, J. B.; Bakken, V.; Adamo, C.; Jaramillo, J.; Gomperts, R.; Stratmann, R. E.; Yazyev, O.; Austin, A. J.; Cammi, R.; Pomelli, C.; Ochterski, J. W.; Ayala, P. Y.; Morokuma, K.; Voth, G. A.; Salvador, P.; Dannenberg, J. J.; Zakrzewski, V. G.; Dapprich, S.; Daniels, A. D.; Strain, M. C.; Farkas, O.; Malick, D. K.; Rabuck, A. D.; Raghavachari, K.; Foresman, J. B.; Ortiz, J. V.; Cui, Q.; Baboul, A. G.; Clifford, S.; Cioslowski, J.; Stefanov, B. B.; Liu, G.; Liashenko, A.; Piskorz, P.; Komaromi, I.; Martin, R. L.; Fox, D. J.; Keith, T.; Al-Laham, M. A.; Peng, C. Y.; Nanayakkara, A.; Challacombe, M.; Gill, P. M. W.; Johnson, B.; Chen, W.; Wong, M. W.; Gonzalez, C.; Pople, J. A. Gaussian 03, Revision C.02, Gaussian, Inc.: Wallingford CT, 2004.
(20) Deng, W.; Cheeseman, J. R.; Frisch, M. J. *J. Chem. Theory Comput.* **2006**, *2*, 1028−1037.
(21) (a) Sychrovský, V.; Gräfenstein, J.; Cremer, D. *J. Chem. Phys.* **2000**, *113*, 3530−3547. (b) Helgaker, T.; Watson, M.; Handy, N. C. *J. Chem. Phys.* **2000**, *113*, 9402−9409. (c) Peralta, J. E.; Scuseria, G. E.; Cheeseman, J. R.; Frisch, M. J. *Chem. Phys. Lett.* **2003**, *375*, 452−458.
(22) López-Vallejo, F.; Fragoso-Serrano, M.; Suárez-Ortiz, G. A.; Hernández-Rojas, A. C.; Cerda-García-Rojas, C. M.; Pereda-Miranda, R. *J. Org. Chem.* **2011**, *76*, 6057−6066.
(23) Tomasi, J.; Cammi, R.; Mennucci, B.; Cappelli, C.; Corni, S. *Phys. Chem. Chem. Phys.* **2002**, *4*, 5697−5712.
(24) MestreLab Research, Santiago de Compostela 15706, Spain, http://mestrelab.com/, accessed on April 21, 2014.
(25) Morris, G. M.; Goodsell, D. S.; Halliday, R. S.; Huey, R.; Hart, W. E.; Belew, R. K.; Olson, A. J. *J. Comput. Chem.* **1998**, *19*, 1639−1662.
(26) Shanker, N.; Kingston, D. G.; Ganesh, T.; Yang, C.; Alcaraz, A. A.; Geballe, M. T.; Banerjee, A.; McGee, D.; Snyder, J. P.; Bane, S. *Biochemistry* **2007**, *46*, 11514−11527.
(27) Löwe, J.; Li, H.; Downing, K. H.; Nogales, E. *J. Mol. Biol.* **2001**, *313*, 1045−1057.
(28) (a) Nettles, J. H.; Li, H.; Cornett, B.; Krahn, J. M.; Snyder, J. P.; Downing, K. H. *Science* **2004**, *305*, 866−869. (b) Nogales, E.; Wolf, S. G.; Downing, K. H. *Nature* **1998**, *391*, 199−203.
(29) (a) Barbier, P.; Dorleans, A.; Devred, F.; Sanz, L.; Allegro, D.; Alfonso, C.; Knossow, M.; Peyrot, V.; Andreu, J. M. *J. Biol. Chem.* **2010**, *285*, 31672−31681. (b) Nawrotek, A.; Knossow, M.; Gigant, B. *J. Mol. Biol.* **2011**, *412*, 35−42. (c) Ranaivoson, F. M.; Gigant, B.; Berritt, S.; Joullie, M.; Knossow, M. *Acta Crystallogr. Sect. D* **2012**, *68*, 927−934. (d) Prota, A. E.; Bargsten, K.; Zurwerra, D.; Field, J. J.; Díaz, J. F.; Altmann, K. H.; Steinmetz, M. O. *Science* **2013**, *339*, 587−590. (e) Prota, A. E.; Magiera, M. M.; Kuijpers, M.; Bargsten, K.; Frey, D.; Wieser, M.; Jaussi, R.; Hoogenraad, C. C.; Kammerer, R. A.; Janke, C.; Steinmetz, M. O. *J. Cell Biol.* **2013**, *200*, 259−270.
(30) Sanner, M. J. *J. Mol. Graphics Mod.* **1999**, *17*, 57−61.
(31) Gasteiger, J.; Marsili, M. *Tetrahedron* **1980**, *36*, 3219−3228.
(32) Trott, O.; Olson, A. J. *J. Comput. Chem.* **2010**, *31*, 455−461.
(33) Morris, G. M.; Huey, R.; Lindstrom, W.; Sanner, M. F.; Belew, R. K.; Goodsell, D. S.; Olson, A. J. *J. Comput. Chem.* **2009**, *16*, 2785−2791.
(34) (a) Plaza, A.; Keffer, J. L.; Bifulco, G.; Lloyd, J. R.; Bewley, C. A. *J. Am. Chem. Soc.* **2010**, *132*, 9069−9077. (b) Meyer, B.; Peters, T. *Angew. Chem., Int. Ed.* **2003**, *42*, 864−890.
(35) Jiménez-Barbero, J.; Canales, A.; Northcote, P. T.; Buey, R. M.; Andreu, J. M.; Díaz, J. F. *J. Am. Chem. Soc.* **2006**, *128*, 8757−8765.
(36) (a) Hess, B.; Kutzner, C.; van der Spoel, D.; Lindahl, E. *J. Chem. Theory Comput.* **2008**, *4*, 435−447. (b) van der Spoel, D.; Lindahl, E.; Hess, B.; Groenhof, G.; Mark, A. E.; Berendsen, H. J. C. *J. Comput. Chem.* **2005**, *26*, 1701−1719. (c) Lindahl, E.; Hess, B.; van der Spoel, D. *J. Mol. Mod.* **2001**, *7*, 306−317. (d) Berendsen, H. J. C.; van der Spoel, D.; van Drunen, R. *Comput. Phys. Commun.* **1995**, *91*, 43−56.
(37) van Gunsteren, W. F.; Berendsen, H. J. C. *Groningen molecular simulation (GROMOS) library manual*; BIOMOS b.v.: Groningen, The Netherlands, 1987.
(38) Berendsen, H. J. C.; Postma, J. P. M.; van Gunsteren, W. F.; DiNola, A.; Haak, J. R. *J. Chem. Phys.* **1984**, *81*, 3684−3690.
(39) Parrinello, M.; Rahman, A. *J. Appl. Phys.* **1981**, *52*, 7182−7190.
(40) Melchionna, S.; Falconi, M.; Desideri, A. *J. Chem. Phys.* **1998**, *108*, 6033−6041.
(41) Svensson, M.; Humbel, S.; Froese, R. D. J.; Matsubara, T.; Sieber, S.; Morokuma, K. *J. Phys. Chem.* **1996**, *100*, 19357−19363.
(42) (a) van Aalten, D. M. F.; Bywater, R.; Findlay, J. B. C.; Hendlich, M.; Hooft, R. W. W.; Vriend, G. *J. Comput. Aided Mol. Design* **1996**, *10*, 255−262. (b) Schuettelkopf, A. W.; van Aalten, D. M. F. *Acta Crystallogr.* **2004**, *D60*, 1355−1363.
(43) Toukan, K.; Rahman, A. *Phys. Rev. B* **1985**, *31*, 2643−2648.
(44) Essmann, U.; Perera, L.; Berkowitz, M. L.; Darden, T.; Lee, H.; Pedersen, L. G. *J. Chem. Phys.* **1995**, *103*, 8577−8592.
(45) (a) Nosé, S. *Mol. Phys.* **1984**, *52*, 255−268. (b) Nosé, S.; Klein, M. L. *Mol. Phys.* **1983**, *50*, 1055−1076.
(46) Hoover, W. G. *Phys. Rev. A* **1985**, *31*, 1695−1697.
(47) Humphrey, W.; Dalke, A.; Schulten, K. *J. Mol. Graphics* **1996**, *14*, 33−38.
(48) Frisch, M. J.; Trucks, G. W.; Schlegel, H. B.; Scuseria, G. E.; Robb, M. A.; Cheeseman, J. R.; Scalmani, G.; Barone, V.; Mennucci, B.; Petersson, G. A.; Nakatsuji, H.; Caricato, M.; Li, X.; Hratchian, H. P.; Izmaylov, A. F.; Bloino, J.; Zheng, G.; Sonnenberg, J. L.; Hada, M.; Ehara, M.; Toyota, K.; Fukuda, R.; Hasegawa, J.; Ishida, M.; Nakajima, T.; Honda, Y.; Kitao, O.; Nakai, H.; Vreven, T.; Montgomery, J. A., Jr.; Peralta, J. E.; Ogliaro, F.; Bearpark, M.; Heyd, J. J.; Brothers, E.; Kudin,

K. N.; Staroverov, V. N.; Kobayashi, R.; Normand, J.; Raghavachari, K.; Rendell, A.; Burant, J. C.; Iyengar, S. S.; Tomasi, J.; Cossi, M.; Rega, N.; Millam, N. J.; Klene, M.; Knox, J. E.; Cross, J. B.; Bakken, V.; Adamo, C.; Jaramillo, J.; Gomperts, R.; Stratmann, R. E.; Yazyev, O.; Austin, A. J.; Cammi, R.; Pomelli, C.; Ochterski, J. W.; Martin, R. L.; Morokuma, K.; Zakrzewski, V. G.; Voth, G. A.; Salvador, P.; Dannenberg, J. J.; Dapprich, S.; Daniels, A. D.; Farkas, Ö.; Foresman, J. B.; Ortiz, J. V.; Cioslowski, J.; Fox, D. J. Gaussian 09, Revision A.1, Gaussian, Inc.: Wallingford, CT, 2009.